Ciência e Agrotecnologia, 42(3):240-247, May/Jun. 2018
http://dx.doi.org/10.1590/1413-70542018423008218

Image analysis to qualify soil erodibility into a wind tunnel

Análise de imagem para qualificar a erobibilidade do solo em um túnel vento

Carlos Asensio[1*], Emilio Rodríguez-Caballero[1], Francisco Jesús García-Navarro[2], José Antonio Torres[3]

[1]University of Almeria, Department of Agronomy, Almeria, Spain
[2]University of Castilla-La Mancha, Department of Science and Technology, Agroforestry and Genetics, Ciudad Real, Spain
[3]University of Almeria, Department of Computer Science, Almeria, Spain
*Corresponding author: casensio@ual.es
Received in April 6, 2017 and approved in June 21, 2018

ABSTRACT

A wind erosion research was carried out in a wind tunnel where sediment samples acquired were studied by an artificial vision camera. These images could be enlarged for further analysis. Image analyses were mainly colorimetry, number of particles present and their size. Soil wind erodibility was analyzed with the image analyses supported by other laboratory results. Anthrosols were the most erodible soils, whereas Calcisols showed the highest resistance to the erosive action of wind. Sediment characteristics show the influence of trap height with decreasing particle size, number and darkness as transport height increases. A two-factor ANOVA for main effect height showed that there were significant differences in particle number and size for sediments trapped 0-15 cm and 40-70 cm high. Soils could be grouped by differences in particle number and size at different heights into highly erodible Anthrosols and Leptosols, non-erodible Calcisols and Arenosols, in which fine particles were already depleted by natural wind erosion. Aggregation showed a similar pattern with decreasing values from Calcisols and Leptosols to Anthrosols and finally Arenosols, where only single sand grains were observed in adhesive traps.

Index terms: Artificial vision camera; soil fertility; semiarid environment.

RESUMO

Um estudo de erosão eólica foi realizado em um túnel de vento, onde amostras de sedimentos foram estudadas por uma câmera de visão artificial. Essas imagens podem ser ampliadas para análise posterior. As análises de imagens foram principalmente colorimetria, número de partículas presentes e seu tamanho. A erodibilidade do vento no solo foi analisada com as análises de imagens em função de outros resultados laboratoriais. Antrossolos foram os solos mais erodíveis, enquanto Calcissolos mostrou a maior resistência à ação erosiva do vento. As características do sedimento mostram a influência da altura da armadilha com a diminuição do tamanho, número e escuridão da partícula à medida que a altura do transporte aumenta. Uma ANOVA de dois fatores para altura do efeito principal mostrou que houve diferenças significativas no número e tamanho de partículas para sedimentos entre 0-15 cm e 40-70 cm de altura. Os solos podem ser agrupados por diferenças no número de partículas e tamanho em diferentes alturas em Antrossolos e Leptossolos altamente erodíveis, Calcissolos e Arenossolos não erodíveis, nos quais as partículas finas já estavam esgotadas pela erosão natural do vento. A agregação apresentou um padrão similar com valores decrescentes de Calcissolos e Leptossolos para Antrossolos e, finalmente, Arenossolos, onde apenas grãos de areia foram observados em armadilhas adesivas.

Termos para indexação: Câmera de visão artificial; fertilidade do solo; ambiente semiárido.

INTRODUCTION

Wind erosion is a global environmental concern with special relevance in agricultural areas around the world (Buschiazzo et al., 2007). Soil resistance to the erosive force of wind mainly depends on vegetation coverage and soil surface properties, such as aggregate stability, structure and texture (Tatarko, 2001; Udo; Takewaka, 2007; Zamani; Mahmoodabadi, 2013). Once wind velocity exceeds the threshold friction capacity of the soil surface, it causes winnowing of soil particles, organic matter, and nutrients (Okin; Gillette, 2001; Okin; Gillette; Herrick, 2006), reducing soil fertility (Li et al., 2007), promoting soil degradation (Zhao et al., 2006) and negatively affecting the vegetation they support (Novara et al., 2011).

Wind erosion can be diminished by vegetation barriers, which trap sediments (Leenders; Sterk; Van Boxel, 2011; Lozano el al., 2013), however the design and evaluation of wind erosion control techniques requires a detailed understanding of detachment and transport processes. Three different modes of soil particle transport by wind have been identified: creep, saltation, and suspension. The finest nutrient-rich particles (<0.001 to 0.1 mm diameter) are subject to long-range transport by suspension, affecting global biogeochemical cycles in source and depositional areas (Zhao et al., 2009). Before

deposition elsewhere, these particles absorb, scatter and reflect solar radiation and affect cloud formation and rain chemistry (Atkinson et al., 2013). Larger particles (> 0.5 mm), which are too heavy for the wind to lift up, are dragged over the soil surface by scraping or transported by saltation. This consists of a series of short hops at heights generally below 1 m, and is responsible for soil and nutrient redistribution within the ecosystem, exerting a local control on natural vegetation and crops (Okin; Gillette; Herrick, 2006; Li et al., 2007). Moreover, during transport, soil particles knock against each other and with the soil surface, breaking them up until they become finer. These particles also impact on plant leaves and stems, reducing their productivity and modifying their structure (Zhang et al., 2014)). Dominance of one mechanism or another mainly depends on wind speed, particle and aggregate size, surface roughness, vegetation coverage, or the length of erodible soil in the main wind direction (Zhang et al., 2004; Andreotti; Claudin; Pouliquen, 2010; Kheirabadi et al., 2018) and may have different implications from regional to global scales (Lyles, 1988). However, few studies have linked wind erosion to detailed grain-size fractions in top soil and windblown sediment. One way this could be done is with the image analysis tools that have been widely used for particle counting and detection in many other disciplines (Ahlers; Alexander, 1985; King et al., 2002; Scheres et al., 2008; Ishizu et al., 2008), but rarely applied to wind erosion experiments.

In this study, we examined wind erosion processes at four different study areas characterized by contrasting soil properties and management. We placed special emphasis on image analysis of windblown sediment particle-size fractions to do this, demonstrating that it is a promising, innovative and accurate tool for the analysis of the physical properties of windblown soil.

MATERIAL AND METHODS

This study was conducted at four different sites, with contrasting soil properties, along the NE-SW wind corridor in Almeria in the southeastern Iberian Peninsula (Figure 1): i) An area with intensive agriculture on hortic Anthrosols ($AT_{h;}$ 36°58'52.2"N 2°03'45.2"W), ii) Degraded shrubland under intensive grazing, where soils are mainly very stony eutric Leptosols ($LP_{e,}$ 36°55'37.2"N 2°10'30.7"W), iii) natural shrublands with scant vegetation coverage mainly dominated by very stony haplic Calcisols ($CL_{h,}$ 36°50'55.8"N 2°19'08.9"W), and iv) an area of sand dunes very close to the Mediterranean Sea, in which soils are mainly endosalic Arenosols ($AR_{es,}$ 36°50'55.8"N 2°19'08.9"W). The climate is semiarid thermo-Mediterranean with a mean annual temperature of 18 ºC and annual precipitation of about 250 mm.

Before starting the wind simulation experiments, we collected three soil samples at each study site. These were collected from the upper 5 cm, dried, crushed, and passed through a 2-mm sieve before standard soil analyses. Particle

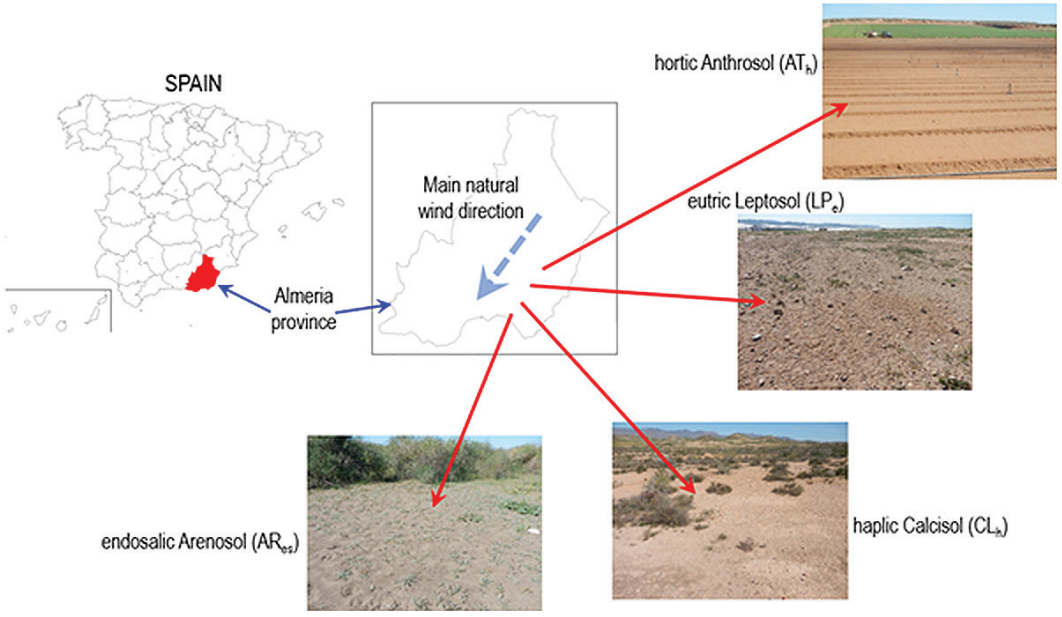

Figure 1: Study area locations.

size distribution was determined by the Robinson pipette method. Organic carbon content (O.C.) was assessed by the Walkley-Black method. Total nitrogen (N) was obtained from NH_3 volumetry. Available soil phosphate (P_2O_5) and available soil potassium (K_2O) were analyzed by photocolorimetry and flame photometry, respectively. Equivalent $CaCO_3$ was found by gas volumetry. Moreover, we used 100-cm^3 cylinders in dry weight determination for bulk density (B.D.).

Wind simulations were conducted using a portable wind tunnel (Figure 2). This tunnel is equipped by a wind generator connected directly to a honeycomb structure that produces a mixed air flow (laminar and turbulent) similar to real conditions. The air flows through a telescopic structure consisting of three different compartments (0.8 x 0.8 x 0.8 m each): i). The first part is structural, equipped with a metal sheet that covers the soil surface to avoid wind erosion in this area. ii) The second compartment represents the study surface, where wind erosion is analyzed, and is equipped with a Next Engine Desktop 3D laser scanner to quantify soil wind erosion as loss of soil thickness. iii) In the third compartment a liquid latex coating was applied to fix soil surface particles. This way, we ensured that wind erosion measured at the end of the tunnel was only produced in the second compartment, where soil surface roughness and subsequent dust deposition was maintained. At the end of the third body of the tunnel, there are four vertical adhesive plates, where transported sediments become attached at heights of 0, 15, 40 and 70 cm.

Five wind simulation experiments were performed in each study area at a wind speed of 6.8 m s^{-1}, which is the maximum daily average wind speed registered at the nearby Nijar weather station (a regional government agriculture weather station). Wind simulation time was set for 5 min, following Fister and Ries (2009), and soil surface was scanned before and after each simulation by the laser scanner.

Soil loss during each wind simulation was estimated using the point clouds acquired by the laser scanner following the methodology proposed by Asensio et al. (2016). Number of particles, size distribution, aggregates and image color histograms of eroded particles trapped by the four vertical adhesive plates were analyzed by means of an artificial vision camera, JAI-CM080 model (5 wind simulations and 3 observations each one: n=15). This is a monochromatic progressive scan camera with a 1024 x 768 pixel resolution connected to a computer which can be used in a way similar to a microscope. Point cloud analysis was done with ArcGIS 10.4 and image analysis was performed in ImageJ. Statistical analyses were done by using SPSS v23 (IBM Corp.).

RESULTS AND DISCUSSION

Physicochemical soil properties before wind simulation experiments at the four different sites are shown in Tables 1 and 2. It may be observed that there is a range of soil textures varying from sandy loam (Calcisols) to sandy soils, with the highest sand content in Arenosols.

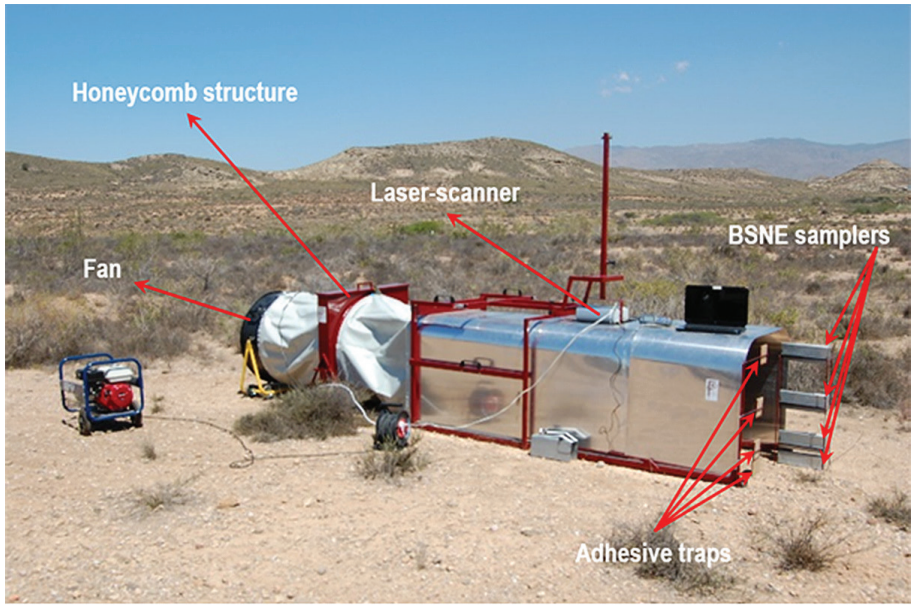

Figure 2: Devices in wind tunnel over a Calcisol.

The very fine sand (100-50 µm) and coarse silt (50-20 µm) fractions, which are the particles most subject to wind erosion transport (Zamani; Mahmoodabadi, 2013), varied from 3.5% to over 30% (Table 1). Gravel, O.C. and $CO_3^=$ content also varied between soil types (Table 2), and this made a strong difference in soil erodibility. Comparison of wind erosion rates in different soils under controlled wind simulation, a proven tool for assessing wind erodibility (Stout; Zobeck, 1996), indicated that the most erodible soils were Anthrosols with erosion rates of about 248±46 g m^{-2} min^{-1}. These soils are subjected to intensive agriculture with frequent tilling, which affects the soil structure and decreases soil surface roughness. Absence of roughness elements on the soil surface, such as macro-aggregates, reduces soil protection and increases wind speed at the soil surface, which finally resulted in higher erosion rates (Zhang et al., 2004). Leptosols showed a higher fraction of easily erodible clay and silt (Table 1), but were less erodible than Anthrosols, with mean erosion rates of 212±40 g m^{-2} min^{-1}. This can be explained by their higher gravel and O.C. content (Table 2). Gravel increases soil surface roughness and hinders wind action on soil surface (Zhang et al., 2004), whereas O.C. favors the formation of stable aggregates that are resistant to erosive agents (Mahmoodabadi; Ahmadbeigi, 2013). Calcisols (Figure 3), which were characterized by high surface stoniness and high carbonate content, which is an important aggregating agent (Barthes et al., 2008), were the least erodible soils with the lowest erosion rate (40±8 g m^{-2} min^{-1}). These values were nearby than observed on similar simulation experiments in Calcisols subjected to ecological agricultural practices (76 g m^{-2} min^{-1}; Asensio et al., 2016) and were within the range of sediment yield values measured on others study areas with high $CaCO_3$ content (Mendez; Buschiazzo, 2010). Arenosols also showed very low erosion rates (66±2 g m^{-2} min^{-1}). This is surprising because of their very low O.C., carbonate and gravel contents, and can be explained by the very low amount of fine particles (Table 1).

Image analysis of transported sediments showed that though there were contrasting differences in soil texture (Table 1), all soils showed a similar pattern with a decreasing number of particles and size as transport height increased (Table 3). The highest number of particles corresponded to coarse particles transported by creep and saltation (Hagen; Van Pelt; Sharratt, 2010). In our wind tunnel design, these particles were trapped at 0 and 15-40 cm high. Only a small fraction of particles were transported by suspension (70 cm high). These were the finest particles and constituted potential runaway dust emissions (Zobeck et al., 2013). Apart from this overall pattern, there were some differences between

Table 1: Textural components in soils.

Sample	% Sand				% Silt			% Clay
	(2000-1000 µm)	(1000-500 µm)	(500-250 µm)	(250-100 µm)	(100-50 µm)	(50-20 µm)	(20-2 µm)	(< 2 µm)
AT_h	5.8 ± 0.4	11.1 ± 0.7	22.6 ± 1.6	31.2 ± 2.7	20.0 ± 1.6	0.4 ± 0.2	2.2 ± 0.3	6.7 ± 0.6
LP_e	15.1 ± 1.2	14.9 ± 0.8	22.4 ± 2.3	24.7 ± .2.1	5.2 ± 0.4	6.4 ± 0.3	2.6 ± 0.3	8.7 ± 0.5
CL_h	6.0 ± 0.6	6.1 ± 0.4	9.5 ± 0.9	19.3 ± 1.8	22.5 ± 2.3	7.5 ± 0.5	11.7 ± 0.9	17.4 ± 1.2
AR_{es}	0.3 ± 0.1	6.1 ± 0.5	48.8 ± 6.4	38.2 ± 3.7	2.9 ± 0.3	0.5 ± 0.2	0.2 ± 0.1	3.0 ± 0.2

Data are means ± standard deviation (n=3).

Table 2: Gravel, organic carbon (O.C.), total nitrogen (N), available phosphorous and potassium (P_2O_5 and K_2O) and equivalent carbonate ($CO_3^=$) content in soils and their bulk density.

Sample	% Gravel	% O.C.	% N	P_2O_5 ($mg \cdot kg^{-1}$)	K_2O ($mg \cdot kg^{-1}$)	% $CO_3^=$	B.D. ($g \cdot cm^{-3}$)
AT_h	5 ± 3	1.70 ± 0.12	0.191 ± 0.012	12 ± 3	7 ± 2	23 ± 4	1.24 ± 0.03
LP_e	37 ± 5	2.54 ± 0.18	0.236 ± 0.064	5 ± 1	16 ± 2	19 ± 3	1.36 ± 0.04
CL_h	22 ± 5	0.90 ± 0.08	0.154 ± 0.014	7 ± 2	8 ± 3	40 ± 6	1.41 ± 0.05
AR_{es}	6 ± 2	1.25 ± 0.07	0.138 ± 0.022	3 ± 1	18 ± 3	1 ± 1	1.28 ± 0.02

Data are means ± standard deviation (n=3).

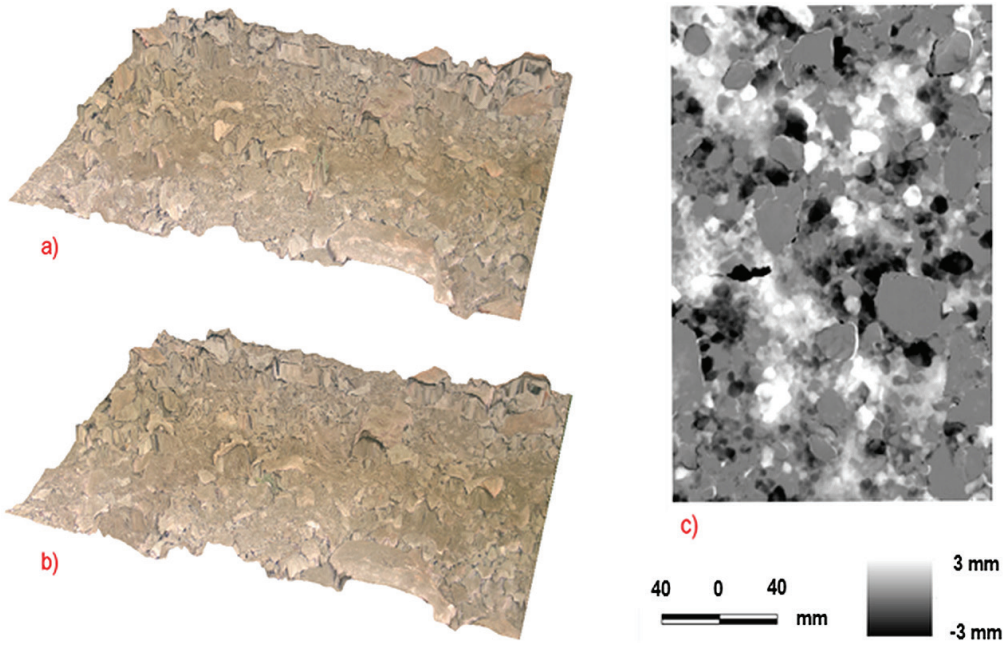

Figure 3: Example of Calcisol surface differences before (a) and after (b) blowing, with its erosion map (c).

Table 3: Number of particles and size in sediment traps with their colorimetric study.

Sample	Particles per observation	Size of particles (mm)	Color		
			Red channel	Green channel	Blue channel
AT-0	41 ± 5	0.56 ± 0.15	53.4 ± 18.3	42.1 ± 17.3	43.4 ± 13.7
AT-15	36 ± 3	0.41 ± 0.11	57.9 ± 17.2	47.4 ± 15.4	48.5 ± 11.7
AT-40	28 ± 6	0.26 ± 0.08	88.6 ± 24.1	82.6 ± 24.4	87.2 ± 23.3
AT-70	32 ± 4	0.14 ± 0.05	78.1 ± 20.7	73.9 ± 21.7	80.0 ± 22.1
LP-0	38 ± 8	0.76 ± 0.17	79.3 ± 15.6	71.0 ± 15.0	70.4 ± 13.0
LP-15	30 ± 6	0.62 ± 0.08	59.4 ± 13.5	48.7 ± 13.5	48.0 ± 10.8
LP-40	22 ± 5	0.28 ± 0.05	63.2 ± 13.1	52.6 ± 13.4	51.9 ± 11.2
LP-70	25 ± 3	0.18 ± 0.02	77.9 ± 14.4	68.8 ± 13.9	68.3 ± 12.0
CL-0	20 ± 3	0.95 ± 0.18	63.6 ± 17.5	49.6 ± 16.1	46.8 ± 11.6
CL-15	18 ± 4	0.76 ± 0.09	62.0 ± 15.0	49.3 ± 14.2	47.9 ± 10.8
CL-40	14 ± 2	0.38 ± 0.08	59.8 ± 14.5	48.7 ± 14.0	48.0 ± 11.0
CL-70	15 ± 2	0.25 ± 0.04	75.2 ± 14.7	70.2 ± 15.4	74.4 ± 15.6
AR-0	31 ± 5	0.55 ± 0.16	41.7 ± 15.8	36.4 ± 16.3	41.1 ± 13.7
AR-15	32 ± 3	0.50 ± 0.13	48.7 ± 14.0	44.9 ± 13.9	51.5 ± 11.8
AR-40	20 ± 2	0.28 ± 0.08	49.8 ± 18.6	45.6 ± 18.5	51.0 ± 15.5
AR-70	16 ± 2	0.22 ± 0.03	63.9 ± 16.6	62.5 ± 18.3	69.6 ± 18.5

Data are means ± standard deviation (n=15).

soils as consequence of the differences in soil erodibility and physicochemical properties (Table 3). According to the two-factor ANOVA, there were three different soil groups: Arenosols, in which fine directly related to suspended particles during wind tunnel experiments (Mirzamostafa, et al., 1998) were already depleted by frequent wind erosion and were characterized by less than 40 particles at all heights, non-erodible Calcisols with less than 20 particles per plate, most of them coarse aggregates attached to plates at 0 and 15 cm high, and highly erodible Anthrosols and Leptosols with more particles attached at all heights. In this last group, it is worth mentioning that particles transported from Leptosols were coarser than those in Anthrosols, mainly because of the higher O.C. content and subsequent aggregation capacity of the first (Mahmoodabadi; Ahmadbeigi, 2013). As shown by Asensio et al. (2015), in wind processes, bulk density tends to maintain a balance between reduction by organic enrichment, and increase by accumulation of fine materials. Zhao et al. (2009) found a very good correlation coefficient of 0.95 between clay and organic matter content in wind transported sediments in China.

We also found some differences in soil particle color between soils and height. Overall particle darkness decreased as transport height increased (Table 3). As particles trapped at 70 cm are subject to long-range transport by suspension before deposition, they increase atmosphere albedo, reducing incoming solar radiation (Atkinson et al., 2013), whereas soils become darker and warmer, modifying most biogeochemical cycles and microbial activity (Maestre et al., 2013). Similar to what was observed during particle size and quantity analysis, soil particle color distribution also varied with the three main groups, Anthrosols/ Leptosols, Calcisols and Arenosols. As an example, color histograms for a Calcisol on plates at 15 and 70 cm high are shown in Figure 4. Table 3 shows the number of particles on adhesive plate traps and their size with their colorimetric study for different soil types and trap height. These results imply that Anthrosols, Leptosols and Calcisols vary in color depending on chromogenic elements present (mainly clay and iron oxides) compared to darker Arenosols, mainly due to their lithological origin.

As showed by Andreotti, Claudin and Pouliquen (2010) sediment flux of sand grains exponentially increases until saturation at longer lengths than these analyzed by us. Thus, higher sediment fluxes could be expected in all soils for wind simulations considering longer bed lengths (Kheirabadi et al., 2018). We can made a comparison in between different soil types behavior, but these absolute values should be taken with care as length of analyzed area may affect saltation process, as well as the fraction of suspended-size aggregates created by abrasion and breakdown of salting aggregates and these effects will vary depending on soil texture and aggregates properties (Mirzamostafa et al., 1998; Kheirabadi et al., 2018).

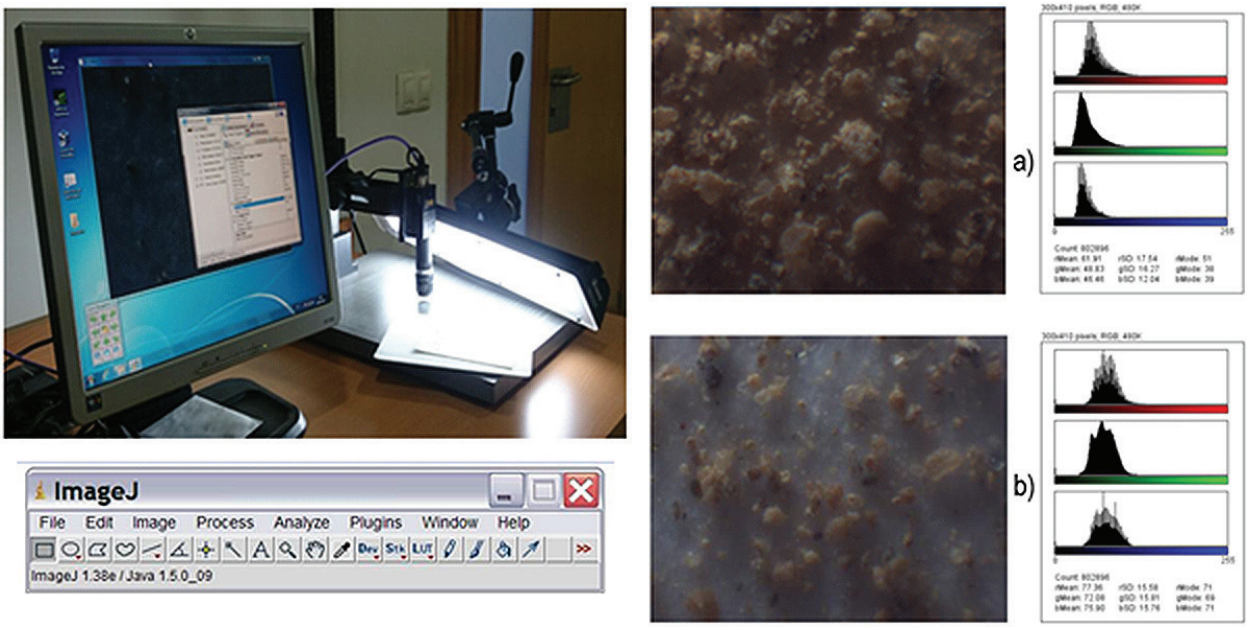

Figure 4: Colorimetric study of a Calcisol in samples at 15 (a) and 70 (b) cm high plates.

CONCLUSIONS

Our results demonstrate that soil physicochemical properties controlled soil resistance to wind erosion. The highest wind erosion rates were found on Anthrosols, which are subjected to intensive agriculture. Degraded Leptosols were also highly erodible, whereas Calcisols showed the lowest erosion rates, because of the aggregating power of their high carbonate content. Arenosols have very low carbonate and organic carbon content, but the small amount of fine particles resulted in very low erosion rates, similar to Calcisols. Image analysis of sediments attached to plates, at different heights at the end of a wind tunnel, offers accurate, high resolution information on particle size distribution and color and has proven to be a useful tool for submillimeter particle counting, size and color analysis. This could enable the creation of a soil database with objectively measurable visual characteristics in the mid-term. The ratio of particle sizes removed by the wind, as a function of trap height, showed two clear blocks: thicker and darker particles displaced by creep and saltation (0 and 15 cm high); and clear, light fine particles displaced by saltation and suspension (40 and 70 cm high).

REFERENCES

AHLERS, K. D.; ALEXANDER, D. R. Microcomputer based digital image processing system developed to count and size laser-generated small particle images. **Optical Engineering**, 24(6):1060-1065, 1985.

ANDREOTTI, B.; CLAUDIN, P.; POULIQUEN, O. Measurements of the aeolian sand transport saturation length. **Geomorphology**, 123:343-348, 2010.

ASENSIO, C. et al. Study on the effectiveness of an agricultural technique based on aeolian deposition, in a semiarid environment. **Environmental Engineering and Management Journal**, 14(5):1143-1150, 2015.

ASENSIO, C. et al. Soil wind erosion in ecological olive trees in the Tabernas desert (Southeastern Spain): A wind tunnel experiment. **Solid Earth**, 7:1233-1242, 2016.

ATKINSON, J. D. et al. The importance of feldspar for ice nucleation by mineral dust in mixed-phase clouds. **Nature**, 498(7454):355-358, 2013.

BARTHES, B. G. et al. Texture and sesquioxide effects on water stable aggregates and organic matter in some tropical soils. **Geoderma**, 143:14-25, 2008.

BUSCHIAZZO, D. E.; ZOBECK, T. M.; ABASCAL, S. A. Wind erosion quantity and quality of an Entic Haplustoll of the semi-arid pampas of Argentina. **Journal of Arid Environments**, 69:29-39, 2007.

FISTER, W.; RIES, J. B. Wind erosion in the central Ebro Basin under changing land use management. Field experiments with a portable wind tunnel. **Journal of Arid Environments**, 73:996-1004, 2009.

HAGEN, L. J.; VAN PELT, S.; SHARRATT, B. Estimating the saltation and suspension components from field wind erosion. **Aeolian Research**, 1:147-153, 2010.

ISHIZU, K. et al. Image processing of particle detection for asbestos qualitative analysis support method -particle counting by using color variance of background. **IEEE** p.3202, 2008.

KHEIRABADI, H. et al. Sediment flux, wind erosion and net erosion influenced by soil bed length, wind velocity and aggregate size distribution. **Geoderma**, 323:22-30, 2018.

KING, M. A. et al. Particle detection, number estimation, and feature measurement in gene transfer studies: Optical fractionator stereology integrated with digital image processing and analysis. **Methods**, 28(2):293-299, 2002.

LEENDERS, J. K.; STERK, G.; VAN BOXEL, J. H. Modelling wind-blown sediment transport around single vegetation elements. **Earth Surface Processes and Landforms**, 36(9):1218-1229, 2011.

LI, J. et al. Quantitative effects of vegetation cover on wind erosion and soil nutrient loss in a desert grassland of southern New Mexico, USA. **Biogeochemistry**, 85:317-332, 2007.

LOZANO, F. J. et al. The influence of blowing soil trapped by shrubs on fertility in Tabernas district (SE Spain). **Land Degradation & Development**, 24:575-581, 2013.

LYLES, L. Basic Wind erosion Processes. **Agriculture, Ecosystems and Environment**, 22/23:91-101, 1988.

MAESTRE, F. T. et al. Changes in biocrust cover drive carbon cycle responses to climate change in drylands. **Global Change Biology**, 19:3835-3847, 2013.

MAHMOODABADI, M.; AHMADBEIGI, B. Dry and water-stable aggregates in different cultivation systems of arid region soils. **Arabian Journal of Geosciences**, 6:2997-3002, 2013.

MENDEZ, M. J.; BUSCHIAZZO, D. E. Wind erosion risk in agricultural soils under different tillage systems in the semiarid Pampas of Argentina. **Soil & Tillage Research**, 106:311-316, 2010.

MIRZAMOSTAFA, N. et al. Soil and aggregate texture effects on suspension components from wind erosion. **Soil Science Society of America Journal**, 62(5):1351-1361, 1998.

NOVARA, A. et al. Soil erosion assessment on tillage and alternative soil managements in a Sicilian vineyard. **Soil & Tillage Research**, 117:140-147, 2011.

OKIN, G. S.; GILLETTE, D. A. Distribution of vegetation in wind-dominated landscapes: Implications for wind erosion modeling and landscape processes. **Journal of Geophysical Research**, 106:9673-9683, 2001.

OKIN, G. S.; GILLETTE, D. A.; HERRICK, J. E. Multi-scale controls on and consequences of aeolian processes in landscape change in arid and semi-arid environments, **Journal of Arid Environments**, 65:253-275, 2006.

SCHERES, S. H. W. et al. Image processing for electron microscopy single-particle analysis using XMIPP. **Nature Protocols**, 3(6):977-990, 2008.

STOUT, J. E.; ZOBECK, T. M. The Wolfforth field experiment: A wind erosion study. **Soil Science**, 161:616-632, 1996.

TATARKO, J. Soil aggregation and win erosion: Processes and measurements. **Annals of Arid Zone**, 40(3):251-263, 2001.

UDO, K.; TAKEWAKA, S. Experimental study of blown sand in a vegetated area. **Journal of Coastal Research**, 23(5):1175-1182, 2007.

ZAMANI, S.; MAHMOODABADI, M. Effect of particle-size distribution on wind erosion rate and soil erodibility. **Archives of Agronomy and Soil Science**, 59(12):1743-1753, 2013.

ZHANG, C. L. et al. Aerodynamic roughness of cultivated soil and its influences on soil erosion by wind in a wind tunnel. **Soil & Tillage Research**, 75:53-59, 2004.

ZHANG, K. et al. Wind tunnel simulation of windblown sand along China's Qinghai-Tibet railway. **Land Degradation & Development**, 25(3):244-250, 2014.

ZHAO, H. L. et al. Wind erosion and sand accumulation effects on soil properties in Horqin Sandy Farmland, Inner Mongolia. **Catena**, 65:71-79, 2006.

ZHAO, H. L. et al. Effects of desertification on soil organic C and N content in sandy farmland and grassland of Inner Mongolia. **Catena**, 77:187-191, 2009.

ZOBECK, T. M. et al. Soil property effects on wind erosion of organic soils. **Aeolian Research**, 10:43-51, 2013.